Frontiers of Information Technology & Electronic Engineering
www.jzus.zju.edu.cn; engineering.cae.cn; www.springerlink.com
ISSN 2095-9184 (print); ISSN 2095-9230 (online)
E-mail: jzus@zju.edu.cn

A novel method for extending the output power back-off range of an asymmetrical Doherty power amplifier*

Mingyu LI[1], Xiaobing CHENG[1], Zhijiang DAI[†‡1], Kang ZHONG[1], Tianfu CAI[1], Chaoyi HUANG[2]

[1]*School of Microelectronics and Communication Engineering, Chongqing University, Chongqing 400044, China*

[2]*School of Optoelectronic Engineering, Chongqing University of Posts and Telecommunications, Chongqing 400065, China*

[†]E-mail: daizj_ok@126.com

Received June 7, 2022; Revision accepted Oct. 7, 2022; Crosschecked Dec. 6, 2022

Abstract: A novel method is proposed to extend the output power back-off (OPBO) range of the Doherty power amplifier (DPA). This study reveals that the OPBO range of the DPA can be extended by tuning the output impedance of the peaking stage away from infinity and changing the phase delay of the output matching network of the carrier power amplifier. Based on this theory, a large-OPBO-range high-efficiency asymmetrical DPA working band from 1.55 to 2.2 GHz (35% relative bandwidth) is designed to verify the proposed method. Experimental results show that the DPA operates from 1.6 to 2.1 GHz. The range of the measured efficiency is 42.2%–52.1% in the OPBO state and 47%–62.7% in the saturation state. The OPBO range is 11.1–13.2 dB.

Key words: Doherty power amplifier (DPA); Output power back-off (OPBO); Output impedance; Network phase
https://doi.org/10.1631/FITEE.2200250 **CLC number:** TN722

1 Introduction

The rapid development of wireless communication systems has changed our lives. Five-generation wireless communication (5G) is characterized by high data rate, massive connections, and low latency. The fast communication of 5G between smart mobile devices gives users an excellent experience (Wei et al., 2014; Liu et al., 2020; Li M et al., 2022). Therefore, wireless communication systems have higher and higher data transmission rate requirements (Koenig et al., 2013). There are two ways to increase the transmission rate of a wireless communication system. One is to improve spectrum utilization (Kliks et al., 2020), and the other is to increase spectrum bandwidth (Tan et al., 2020). The most used modulation technique is orthogonal frequency division multiplexing (OFDM) to increase spectrum utilization, which will cause a larger signal peak-to-average power ratio (PAPR) (Vijarnstit et al., 2015). OFDM signals can reach the PAPR level of 8–12 dB. Therefore, improving the efficiency of the amplifier in the output power back-off (OPBO) state is beneficial to improving the overall performance of the transmitter system (Darraji et al., 2011). Power amplifiers with a high OPBO (Fang and Cheng, 2014; Hallberg et al., 2016) range have become a research hotspot in recent years (Zhou et al., 2018).

Efficiency enhancement technology in the OPBO state includes envelope tracking technology (Lee SC et al., 2015), outphasing technology (Chung et al., 2018; Sen, 2018), envelope elimination and restoration (EER) technology (Bolotov et al., 2018), and Doherty architecture power amplifier technology. The structures of envelope tracking technology, outphasing technology, and EER technology are very complex and difficult to realize (Mustafa et al., 2009;

‡ Corresponding author
* Project supported by the National Natural Science Foundation of China (Nos. 62001061 and 62171068), the Science and Technology Research Program of Chongqing Municipal Education Commission (No. KJQN201900621), and the Natural Science Foundation of Chongqing, China (No. cstc2020jcyj-msxmX0129)
ORCID: Zhijiang DAI, https://orcid.org/0000-0003-4914-1464
© Zhejiang University Press 2023

Cidronali et al., 2013; Tajima et al., 2017; de Falco et al., 2018). Compared to other technologies, the Doherty power amplifier (DPA) has low complexity and strong applicability for broadband signals (Kim et al., 2006), so DPA is suitable for engineering applications. DPA architecture has evolved into different types, such as symmetric DPA (Özen et al., 2016; Hasin and Kitchen, 2019; Li C et al., 2020), asymmetric DPA (Fang et al., 2018), three-way Doherty (Suo and Bao, 2008; Lehna and Bangert, 2016), and the dynamic load modulation power amplifier by external active devices (Gustafsson et al., 2013). The dynamic load modulation power amplifier has high design complexity and high realization cost (Andersson et al., 2012). The three-way DPA needs three active devices, so the manufacturing cost will be higher. The OPBO of the traditional symmetric DPA is only 6 dB. Therefore, the OPBO of the symmetric DPA cannot adapt to the high PAPR signal. Compared with the symmetric DPA, the asymmetric DPA can achieve a larger OPBO range.

Therefore, asymmetric DPA has come into our lives. Iwamoto et al. (2001) used gallium arsenide (GaAs) technology to make an asymmetric DPA with a large OPBO range. Lee J et al. (2014) designed a new asymmetric DPA. To increase the gain of the peak power amplifier, it is composed of two single tube power amplifiers. The OPBO of the DPA reached 7 dB. Nghiem and Negra (2014) designed an asymmetric DPA, which operated at 1.85–2.4 GHz and the OPBO reached 10 dB. Pang et al. (2016) designed an asymmetric DPA using asymmetric drain bias voltage. The frequency range was 1.55–2.35 GHz, the OPBO range was 8–9 dB, and the efficiency in the OPBO state was as high as 50.4%–56.2%.

In this study, a new method based on an unbalanced power amplifier is proposed to increase the OPBO range. This method broadens the OPBO range by using non-infinite output impedance of the peak power amplifier and the phase shift of the output matching network of the carrier power amplifier. The output impedance of the peak power amplifier and the phase shift of the output matching network of the carrier power amplifier satisfy a one-to-one relationship. First, the design theory is introduced. Then the effectiveness of the method is verified by simulation and experimental results. Compared with the traditional asymmetric DPA, the asymmetric DPA designed with this method has a larger OPBO range.

2 Extending the OPBO range of the asymmetrical DPA

2.1 Comparison of 6 dB and 12 dB OPBO DPA

The theoretical efficiency of the 6 and 12 dB OPBO DPA is shown in Fig. 1. Fig. 1 shows that the efficiency curve of DPA presents a peak point in the OPBO state and saturation state, respectively. The highest drain efficiency is 78.5% in both the OPBO state and saturation state. When the peak power amplifier is tuned on, the efficiency of DPA decreases until the peak amplifier reaches saturation. For this reason, the efficiency curve forms a pit. The average efficiency is defined in Eq. (1):

$$\mathrm{Eff} = \sum_{i=1}^{n} P(i) \cdot \mathrm{Eff}(i), \tag{1}$$

where Eff represents the average efficiency, Eff(i) represents the efficiency at each output power, and $P(i)$ represents the probability density at each output power. The PAPR of the broadband long-term evolution (LTE) signal is more than 9 dB and even reaches 12 dB in the case of multi-carrier aggregation. The traditional DPA with 6 dB OPBO cannot meet the application requirements. Thus, the DPA with a larger OPBO has more competitive advantages based on Eq. (1).

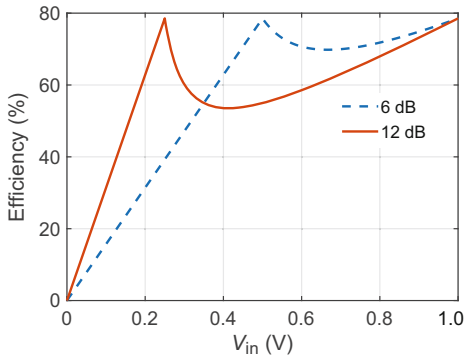

Fig. 1 Theoretical efficiency of the 6 dB and 12 dB output power back-off (OPBO) Doherty power amplifier (DPA)

2.2 Active load modulation of the novel asymmetric DPA

The asymmetric DPA block diagram (Fig. 2) consists of a carrier transistor, a peak transistor, the output matching network of the carrier power amplifier ($\mathrm{OMN_C}$), the output matching network of the peak power amplifier ($\mathrm{OMN_P}$), and the impedance looking into the load from the modulation point (Z_L). I_C and I_P represent the carrier transistor and peak transistor, respectively. R_L and X_L represent the real part and imaginary part of the impedance looking into the load from the modulation point, respectively. As shown in Eq. (2), β represents the ratio of X_L to R_L. As shown in Eq. (3), α represents the ratio of the maximum current of the peak power amplifier ($I_{\mathrm{p\,max}}$) to the maximum current of the carrier power amplifier ($I_{\mathrm{c\,max}}$). Here, $\alpha \neq 1$ due to the asymmetric architecture. Z_CS is the impedance looking into $\mathrm{OMN_C}$ from the carrier transistor in the saturation state, and Z_CB is the impedance looking into $\mathrm{OMN_C}$ from the carrier transistor in the OPBO state. $P_{\mathrm{c_sat}}$ and $P_{\mathrm{c_obo}}$ represent the output power of the carrier power amplifier in the saturation state and OPBO state, respectively. As shown in Eq. (4), n is the ratio of $P_{\mathrm{c_sat}}$ to $P_{\mathrm{c_obo}}$. OPBO can be expressed as Eq. (5). It can be determined that OPBO increases with the increase of n.

$$\beta=\frac{X_\mathrm{L}}{R_\mathrm{L}}, \tag{2}$$

$$\alpha=\frac{I_{\mathrm{p\,max}}}{I_{\mathrm{c\,max}}}, \tag{3}$$

$$n=\frac{P_{\mathrm{c_sat}}}{P_{\mathrm{c_obo}}}, \tag{4}$$

$$\mathrm{OPBO}=10n\lg(1+\alpha). \tag{5}$$

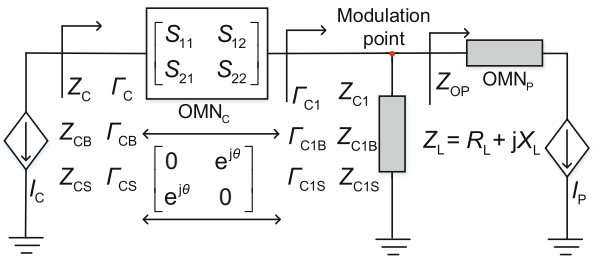

Fig. 2 Block diagram of the asymmetric Doherty power amplifier (DPA)

The scatter parameter matrix of $\mathrm{OMN_C}$ is shown in Fig. 2. $\mathrm{OMN_C}$ represents the output matching network of the carrier power amplifier. $\mathrm{OMN_C}$ matches $(1+\alpha)Z_\mathrm{L}$ to R_opt in the saturation state and $Z_\mathrm{L}//Z_\mathrm{OP}$ to nR_opt in the OPBO state. θ represents the phase delay of $\mathrm{OMN_C}$. Γ_C1S represents the reflection coefficient of port 2 looking into the combining point in the saturation state, and Γ_CS represents the reflection coefficient of the carrier transistor looking into port 1 in the saturation state. Assuming that $\Gamma_\mathrm{C1S}=\Gamma_\mathrm{CS}=0$, the saturation state is well matched. Γ_CB represents the reflection coefficient of the carrier transistor looking into port 1 in the OPBO state. Γ_CB can be expressed as Eq. (6). For the convenience of calculation, the peak power amplifier output impedance (Z_OP) can be expressed as Eq. (7), and variable X is introduced to represent Z_OP.

$$\Gamma_\mathrm{CB}=\frac{-\mathrm{j}\alpha X-1+\mathrm{j}\beta}{\mathrm{j}(2+\alpha)X+1+\mathrm{j}\beta}\mathrm{e}^{\mathrm{j}2\theta}, \tag{6}$$

$$Z_\mathrm{OP}=\mathrm{j}(1+\alpha)XR_\mathrm{L}. \tag{7}$$

After α is determined, Γ_CB is related to X, θ, and β. Assuming that $\alpha=2.5$, Γ_CB can be expressed as Eq. (8). Z_CB can be expressed as Eq. (9). R_opt represents the optimal impedance of a class B amplifier. We can know that n reaches the maximum when β is equal to 0. This means that the asymmetric DPA has the largest OPBO range when the load impedance is a real number.

$$\Gamma_\mathrm{CB}=\frac{-2.5\mathrm{j}X-1+\mathrm{j}\beta}{4.5\mathrm{j}X+1+\mathrm{j}\beta}\mathrm{e}^{\mathrm{j}2\theta}, \tag{8}$$

$$Z_\mathrm{CB}=\frac{1+\Gamma_\mathrm{CB}}{1-\Gamma_\mathrm{CB}}R_\mathrm{opt}. \tag{9}$$

n is determined by Γ_CB. Specifically, n can be expressed as Eq. (10) when Γ_CB is a real number:

$$n=\frac{1+\Gamma_\mathrm{CB}}{1-\Gamma_\mathrm{CB}}. \tag{10}$$

For the proposed DPA, Z_OP is non-infinite and θ is divergent. Z_CB is shown in Fig. 3. The green circle is obtained by scanning θ after X is fixed to infinity. The purple circle is obtained by scanning X after θ is fixed to $-81.5°$. The black point is obtained by fixing X to infinity after θ is fixed to $-90°$. The green point is obtained by letting $Z_\mathrm{OP}=\mathrm{j}R_L$ and $\theta=-81.5°$. For a traditional DPA, Z_CB can be represented by the black point. In this article, Z_CB

falls in the red region. This means that the novel DPA can achieve the largest OPBO range due to the increase of Γ_{CB}.

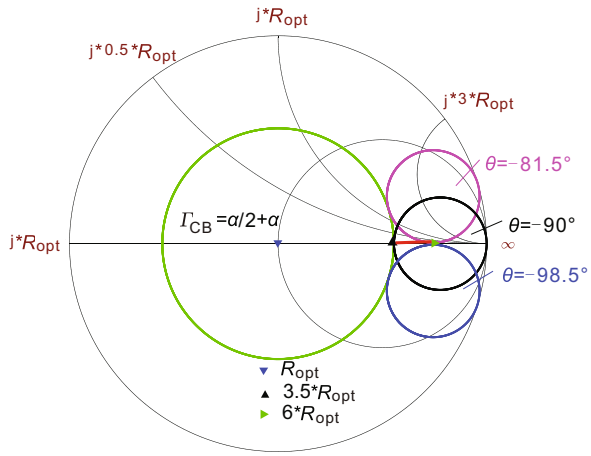

Fig. 3 The load-pull of the carrier transistor (Z_{CB}) (References to color refer to the online version of this figure)

Theoretically, if $\alpha = 2.5$, the range of OPBO is 10.8–13.8 dB. The range of θ is $-81.5°$ to $-98.5°$. In addition, θ and Z_{OP} have a one-to-one correspondence. For example, if $Z_{\mathrm{OP}} = \mathrm{j}R_{\mathrm{L}}$, OPBO is close to 13.8 dB when $\theta = -81.5°$. If Z_{OP} is infinity, OPBO is close to 10.8 dB when $\theta = -90°$.

3 Design principle of the output matching network

The output matching network of the carrier and peak power amplifier structure diagram is shown in Fig. 4. Carrier and peaking represent the carrier and peak power amplifier, respectively. $\mathrm{OMN_C}$ stands for the output matching network of the carrier power amplifier. $\mathrm{OMN_C}$ not only ensures that the carrier power amplifier is in a good matching state in the power saturation state, but also ensures that it is in a good matching state when it is in the power back-off state. $\mathrm{OMN_P}$ is the output matching network of the peak power amplifier and it is in a good matching state in the power saturation state. Both $\mathrm{OMN_C}$ and $\mathrm{OMN_P}$ contain parasitic parameters. Z_{CS} and Z_{CB} are the impedance looking into $\mathrm{OMN_C}$ from the carrier transistor in the saturation state and OPBO state, respectively. Z_{PS} is the impedance looking into $\mathrm{OMN_P}$ from the peaking transistor in the saturation state.

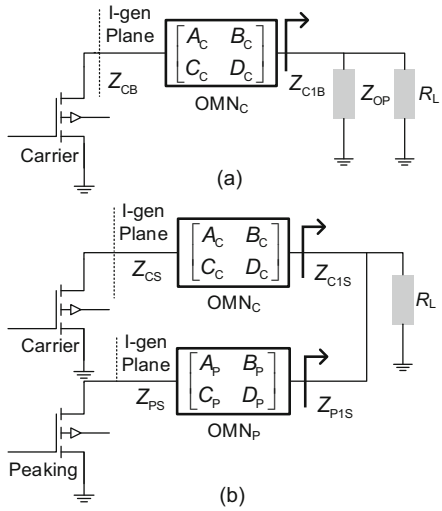

Fig. 4 Output matching network structure diagram of the carrier and peak power amplifier: (a) output power back-off (OPBO) state; (b) saturation state

$$Z_{\mathrm{CS}} = \frac{A_{\mathrm{C}}(1+\alpha)R_{\mathrm{L}} + B_{\mathrm{C}}}{C_{\mathrm{C}}(1+\alpha)R_{\mathrm{L}} + D_{\mathrm{C}}}, \tag{11}$$

$$Z_{\mathrm{PS}} = \frac{A_{\mathrm{P}}(1+\frac{1}{\alpha})R_{\mathrm{L}} + B_{\mathrm{P}}}{C_{\mathrm{P}}(1+\frac{1}{\alpha})R_{\mathrm{L}} + D_{\mathrm{P}}}, \tag{12}$$

$$Z_{\mathrm{CB}} = \frac{A_{\mathrm{C}}(R_{\mathrm{L}}//Z_{\mathrm{OP}}) + B_{\mathrm{C}}}{C_{\mathrm{C}}(R_{\mathrm{L}}//Z_{\mathrm{OP}}) + D_{\mathrm{C}}}. \tag{13}$$

In the power saturation state, the best load impedance of the carrier power amplifier can be represented by $R_{\mathrm{c_opt}}$, and the best load impedance of the peak power amplifier can be represented by $R_{\mathrm{p_opt}}$. In the OPBO state, the best load impedance of the carrier power amplifier can be represented by $[Z_{\mathrm{cb_opt}}]$. That is, the red area in Fig. 3 is represented by $[Z_{\mathrm{cb_opt}}]$.

Optimize the parameters of $\mathrm{OMN_C}$ and $\mathrm{OMN_P}$ and make Z_{CS}, Z_{PS}, and Z_{CB} satisfy Eqs. (14), (15), and (16), respectively. This means that the carrier power amplifier can achieve optimal impedance in both saturation and OPBO states. This also means that the peak amplifier achieves the optimal load impedance in the saturation state.

$$Z_{\mathrm{CS}} \to R_{\mathrm{c_opt}}, \tag{14}$$

$$Z_{\mathrm{PS}} \to R_{\mathrm{p_opt}}, \tag{15}$$

$$Z_{\mathrm{CB}} \to \left[Z_{\mathrm{cb_opt}}\right]. \tag{16}$$

To make Z_{CB} fall into the red region of Fig. 3, it is necessary to make θ decrease linearly from $-81.5°$ to $-98.5°$ and Z_{OP} first increase from $\mathrm{j}R_{\mathrm{L}}$ to infinity and then decrease to $-\mathrm{j}R_{\mathrm{L}}$ with the increase of the frequency. Thus, to satisfy Eq. (16), Eqs. (17) and (18) must be satisfied:

$$\theta \to [\theta_{\mathrm{opt}}]\,, \tag{17}$$

$$Z_{\mathrm{OP}} \to [Z_{\mathrm{OP}}]\,. \tag{18}$$

$[\theta_{\mathrm{opt}}]$ and $[Z_{\mathrm{OP}}]$ are both matrices. The elements in $[\theta_{\mathrm{opt}}]$ linearly decrease from $-81.5°$ to $-98.5°$. The elements in $[Z_{\mathrm{OP}}]$ first increase from $\mathrm{j}R_{\mathrm{L}}$ to infinity and then decrease to $-\mathrm{j}R_{\mathrm{L}}$. E_{rr1} represents the relative error of Z_{CS} and $R_{\mathrm{c_opt}}$. E_{rr2} represents the relative error of Z_{PS} and $R_{\mathrm{p_opt}}$. E_{rr3} represents the relative error of θ and $[\theta_{\mathrm{opt}}]$. E_{rr4} represents the relative error of Z_{OP} and $[Z_{\mathrm{OP}}]$.

$$E_{\mathrm{rr1}} = \frac{\left|Z_{\mathrm{CS}} - R_{\mathrm{c_opt}}\right|}{R_{\mathrm{c_opt}}}, \tag{19}$$

$$E_{\mathrm{rr2}} = \frac{\left|Z_{\mathrm{PS}} - R_{\mathrm{p_opt}}\right|}{R_{\mathrm{p_opt}}}, \tag{20}$$

$$E_{\mathrm{rr3}} = \frac{\left|\theta - [\theta_{\mathrm{opt}}]\right|}{[\theta_{\mathrm{opt}}]}, \tag{21}$$

$$E_{\mathrm{rr4}} = \frac{\left|Z_{\mathrm{OP}} - [Z_{\mathrm{OP}}]\right|}{[Z_{\mathrm{OP}}]}. \tag{22}$$

E_{rr} represents the total error. W_1 represents the weight of the relative error of Z_{CS} and $R_{\mathrm{c_opt}}$. W_2 represents the weight of the relative error of Z_{PS} and $R_{\mathrm{p_opt}}$. W_3 represents the weight of the relative error of θ and $[\theta_{\mathrm{opt}}]$. W_4 represents the weight of the relative error of Z_{OP} and $[Z_{\mathrm{OP}}]$.

$$\begin{aligned} E_{\mathrm{rr}} =& W_1|E_{\mathrm{rr1}}|^2 + W_2|E_{\mathrm{rr2}}|^2 + W_3|E_{\mathrm{rr3}}|^2 \\ &+ W_4|E_{\mathrm{rr4}}|^2. \end{aligned} \tag{23}$$

Adopting some technical means (gradient algorithm, real frequency technology, etc.), optimize the network parameters to make E_{rr} as small as possible. Under this condition, the carrier amplifier obtains the best load impedance in the saturation and OPBO states. The peak amplifier obtains the best load impedance in the saturation state. The algorithm flowchart of design $\mathrm{OMN_C}$ and $\mathrm{OMN_P}$ is shown in Fig. 5.

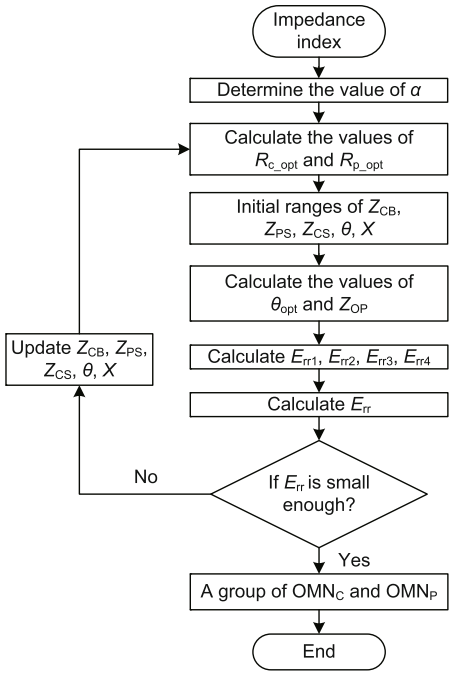

Fig. 5 Algorithm flowchart of design $\mathrm{OMN_C}$ and $\mathrm{OMN_P}$

4 Design of the extended asymmetrical DPA

To verify the above theory, a particular process of the asymmetrical DPA with a large OPBO range is proposed. The schematic of the whole asymmetrical DPA is given in Fig. 6. The working frequency of the asymmetrical DPA is 1.55–2.2 GHz (35% relative bandwidth). In this design, a CGH40010F transistor with a drain voltage of 28 V is used for the carrier power amplifier, and a CGH40045F transistor with a drain voltage of 28 V is used for the peak power amplifier. The substrate is Rogers 4350B. The dielectric constant $\varepsilon = 3.66$ and the thickness $H = 20$ mil. The optimal impedance biased in class B is set as 36 Ω. First of all, set $\alpha = 2.5$ based on the above analysis. Second, for the convenience of design, let $R_{\mathrm{L}} = 15$ Ω.

The main power amplifier is biased at class AB, and the gate voltage is -2.8 V. The input matching network of the carrier power amplifier matches 50 Ω to optimal source impedance. The packaged parameters should be added to $\mathrm{OMN_C}$. The peak power amplifier is biased at class C, and the gate voltage is -5.2 V. The input matching network of the peak power amplifier matches 50 Ω to optimal source impedance. The post matching network (PMN)

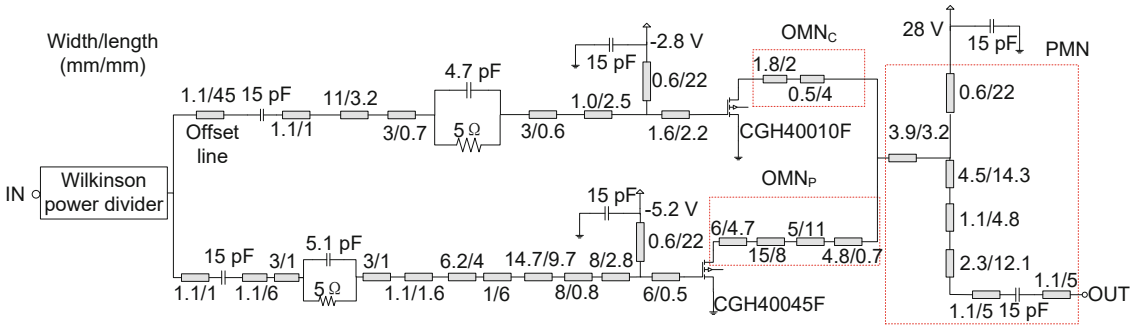

Fig. 6 Schematic of the whole asymmetrical Doherty power amplifier (DPA) (PMN: post matching network)

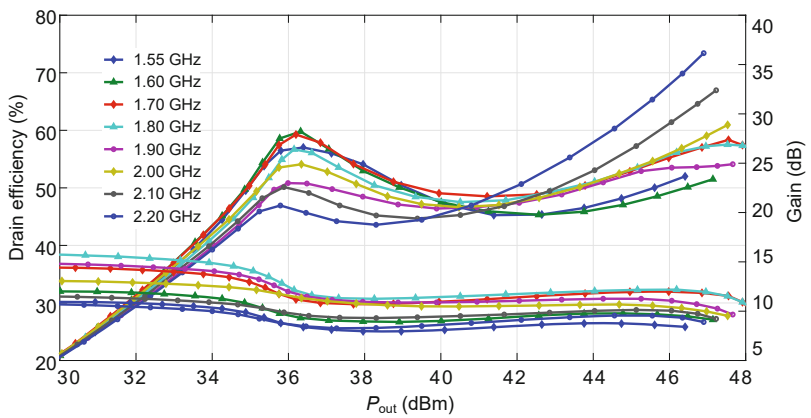

Fig. 7 Simulation results of the asymmetrical Doherty power amplifier (DPA)

matches R_L to 50 Ω throughout the frequency band. This design uses a Wilkinson power divider to divide the input signal into two to satisfy the power demand of the peaking amplifier. The power ratio is set to 2.5:1. The offset line is added to ensure the phase shifts of the carrier and the peak to be consistent.

Fig. 7 shows the simulation results of the asymmetrical DPA. The range of the OPBO is 11.2–12.4 dB over 1.55–2.2 GHz (35% relative bandwidth). The efficiency is 46.8%–57.4% in the OPBO state and 54.1%–73.4% in the saturation state. The gain is 8.9–10.2 dB in the saturation state. The maximum output power is 46.9–48.1 dBm.

5 Experimental results

Fig. 8 is a photograph of the asymmetrical DPA. This asymmetrical DPA has five ports including three direct current (DC) ports and two radio frequency (RF) ports. The DC bias port includes a drain bias port, a carrier power amplifier gate bias port, and a peak power amplifier gate bias port. This asymmetrical DPA has one fewer drain bias port than the conventional DPA. In addition, this asymmetrical DPA has one RF input port and one RF output port.

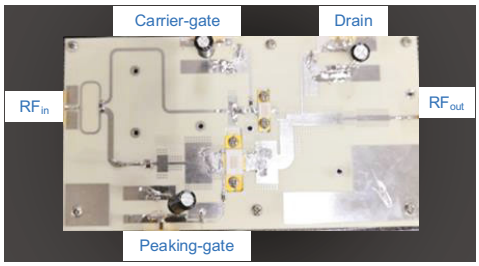

Fig. 8 Photograph of the fabricated asymmetrical Doherty power amplifier (DPA)

Fig. 9 shows the experimental test platform, which is composed of a DC power supply, signal source, driving power amplifier, isolator, asymmetrical DPA, attenuator, and spectrum analyzer. Because the maximum power of the signal source is

not enough to make the asymmetrical DPA work in the saturation state, it is necessary to add a driving power amplifier before the asymmetrical DPA. An isolator is added between the driving power amplifier and the asymmetrical DPA. To protect the spectrometer, a 30 dB attenuator is added in front of the spectrometer. During the test, the gate voltage of the main power amplifier is –2.8 V. The gate voltage of the peak power amplifier is –5.5 V. The drain voltage of the DPA is 28 V.

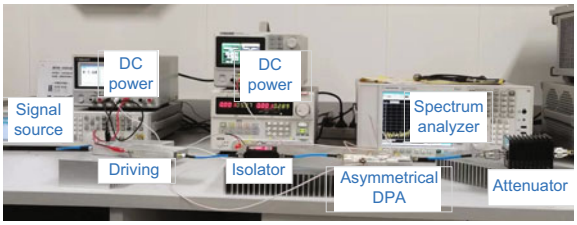

Fig. 9 Photograph of the experimental test platform of the asymmetrical Doherty power amplifier (DPA)

5.1 Measurements under the continuous wave signals

First, the DPA is tested under single-tone continuous wave excitation. The frequency of the signal is 1.6–2.1 GHz with a 100 MHz frequency step. The experimental results of the asymmetrical DPA are shown in Fig. 10. The carrier power amplifier is over saturated when the asymmetrical DPA operates at 2.1 GHz. The maximum output power is 45.2 dBm. The efficiency is 46.5% in the OPBO state and 62.7% in the saturation state. The gain is 5.3 dB in the saturation state. Overall, the experimental results are acceptable when the asymmetrical DPA operates at 1.6–2.1 GHz. The efficiency is 42.2%–52.1% in the OPBO state and 47%–62.7% in the saturation state. The gain is 5.3–7.3 dB in the saturation state. The range of OPBO is 11.1–13.2 dB. The maximum output power is 45.2–47.3 dBm. The experimental results show the DPA operating at 1.6–2.1 GHz (27% relative bandwidth), but the DPA is designed for 1.55–2.2 GHz (35% relative bandwidth). This may be caused by an inaccurate transistor model.

5.2 Measurements under the LTE modulated signals

To prove that the asymmetric DPA can be applied to modern communication systems, the DPA is tested under a continuously modulated wave excitation signal. The PAPR of the LTE modulated signal is 10 dB and the bandwidth is 20 MHz. Digital pre-distortion (DPD) can improve the linearity of the DPA. The Zynq UltraScale + RFSoC evaluation board (ZCU111) of the Xilinx company is used to generate LTE modulation signals and collect and process the output signals of the asymmetric DPA. DPD is realized using the generalized memory polynomial (GMP) model. The core principle is to use the direct learning structure to iterate the coefficients until they converge.

When the center frequency of the LTE modulated signal is 1.8 GHz and the average output power of the asymmetric DPA is about 35.2 dBm, the measured AM-AM and AM-PM curves of the asymmetric DPA with and without DPD are shown in Fig. 11. Fig. 12 shows the measured output spectrum of the asymmetric DPA with and without DPD. The adjacent channel power ratio (ACPR) of the asymmetric DPA before DPD is −27.2/−26.6 dBc. The ACPR of the asymmetric DPA can be improved

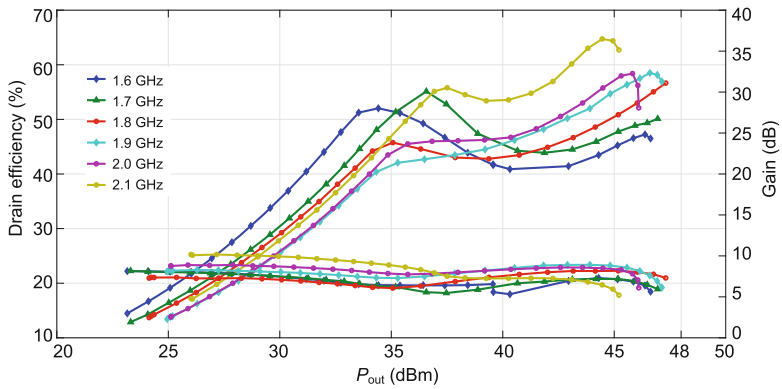

Fig. 10 Experimental results of the asymmetrical Doherty power amplifier (DPA)

to −46.7/−46.4 dBc after DPD. So, the ACPR of the asymmetric DPA is improved by 19.5/19.8 dB through DPD at 1.8 GHz.

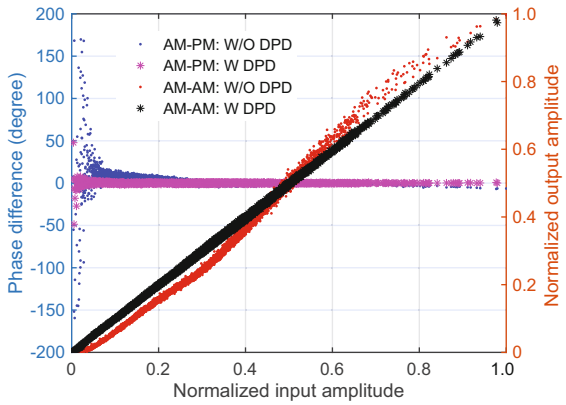

Fig. 11 The measured AM-AM and AM-PM curves of the asymmetric Doherty power amplifier (DPA) with or without digital pre-distortion (DPD) at a center frequency of 1.8 GHz

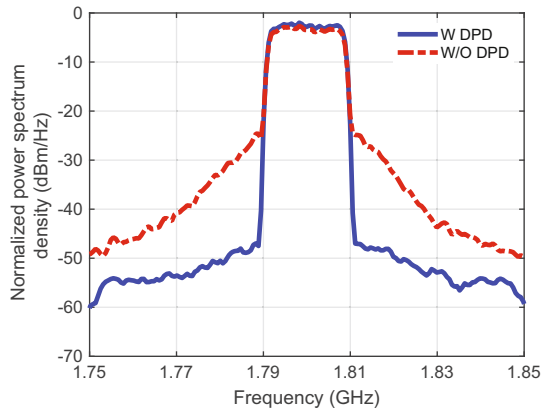

Fig. 12 The measured output spectrum of the asymmetric Doherty power amplifier (DPA) with or without digital pre-distortion (DPD) at a center frequency of 1.8 GHz

Fig. 13 shows the measured AM-AM and AM-PM curves of the asymmetric DPA with and without DPD when the center frequency of the LTE modulated signal is 2 GHz and the average output power of the asymmetric DPA is about 35 dBm. Fig. 14 shows the measured output spectrum of the asymmetric DPA with and without DPD. The ACPR of the asymmetric DPA before DPD is −29.1/−27.6 dBc. The ACPR of the asymmetric DPA can be improved to −43.6/−42.7 dBc after DPD. So, the ACPR of the asymmetric DPA is improved by 14.5/15.1 dB through DPD at 2 GHz.

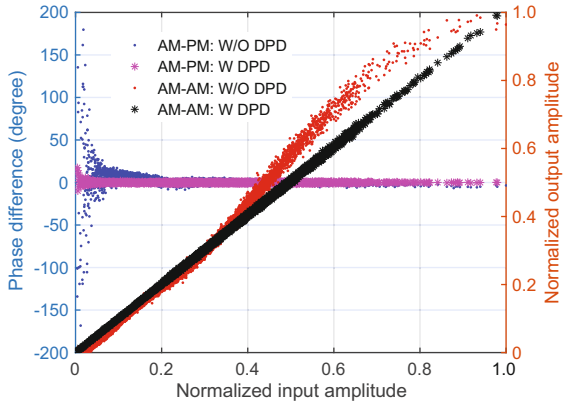

Fig. 13 The measured AM-AM and AM-PM curves of the asymmetric Doherty power amplifier (DPA) with or without digital pre-distortion (DPD) at a center frequency of 2 GHz

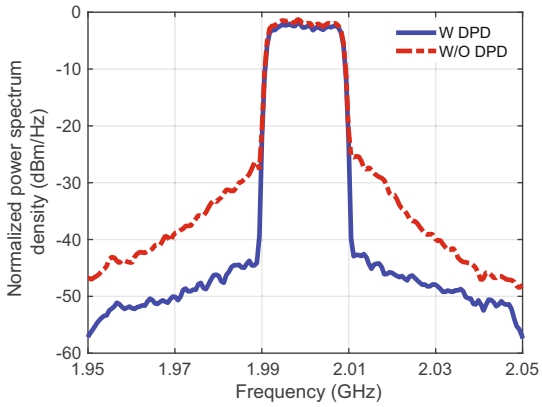

Fig. 14 The measured output spectrum of the asymmetric Doherty power amplifier (DPA) with or without digital pre-distortion (DPD) at a center frequency of 2 GHz

5.3 Performance comparison

Table 1 shows the performance comparison between the asymmetric DPA and other DPAs. As can be seen, the asymmetric DPA has a larger range of OPBO and higher efficiency in the OPBO state than most other DPAs. This shows that the novel method for extending the OPBO range is effective in designing DPAs.

6 Conclusions

This paper presents a method for extending the OPBO range of the DPA. To verify the theory, a novel method of asymmetrical DPA with a large OPBO range is designed. Experimental results show that the designed asymmetric DPA operates at 1.6–2.1 GHz. The OPBO range is 11.1–13.2 dB and the

Table 1 Comparison between our Doherty power amplifier (DPA) and some DPAs in the literature

Reference	Frequency (GHz)	FBW (%)	Power (dBm)	OPBO (dB)	Eff-OPBO (%)	Eff-sat (%)
Özen et al., 2016	1.95	–	44	9	50	–
Hasin and Kitchen, 2019	2.2	–	43.6	9	50.7	71
Li C et al., 2019	1.9–2.4	23.2	44.1–44.8	8.5–9	44.2–49.7	65.2–71.8
Fang et al., 2018	1.35–1.7	22.9	42	9	50–56	71–76
This work	1.6–2.1	27	45.2–47.3	11.1–13.2	42.2–52.1	47–62.7

FBW: fractional bandwidth; OPBO: output power back-off; Eff-OPBO: efficiency in the OPBO state; Eff-sat: efficiency in the saturation state

maximum output power is 45.2–47.3 dBm. The efficiency range is 42.2%–52.1% in the OPBO state and 47%–62.7% in the saturation state. The theory can also be used to develop a symmetrical DPA.

Contributors

Mingyu LI, Xiaobing CHENG, and Zhijiang DAI designed the research. Xiaobing CHENG drafted the paper. Kang ZHONG, Tianfu CAI, and Chaoyi HUANG helped organize the paper. Zhijiang DAI revised and finalized the paper.

Compliance with ethics guidelines

Mingyu LI, Xiaobing CHENG, Zhijiang DAI, Kang ZHONG, Tianfu CAI, and Chaoyi HUANG declare that they have no conflict of interest.

Data availability

The data that support the findings of this study are available from the corresponding author upon reasonable request.

References

Andersson CM, Gustafsson D, Yamanaka K, et al., 2012. Theory and design of class-J power amplifiers with dynamic load modulation. *IEEE Trans Microw Theory Techn*, 60(12):3778-3786. https://doi.org/10.1109/TMTT.2012.2221140

Bolotov AO, Kholyukov RG, Varlamov OV, 2018. EER power amplifier modulator efficiency improvement using PWM with additional sigma-delta modulation. Systems of Signal Synchronization, Generating and Processing in Telecommunications, p.1-4. https://doi.org/10.1109/SYNCHROINFO.2018.8456955

Chung A, Rejeb MB, Darwish A, et al., 2018. Frequency doubler based outphasing system for millimeter wave vector signal generation. 15th European Radar Conf, p.449-452. https://doi.org/10.23919/EuRAD.2018.8546541

Cidronali A, Mercanti M, Giovannelli NÒ, et al., 2013. On the signal probability distribution conscious characterization of GAN devices for optimum envelope tracking PA design. *IEEE Microw Wirel Compon Lett*, 23(7):380-382. https://doi.org/10.1109/LMWC.2013.2262929

Darraji R, Ghannouchi FM, Hammi O, 2011. A dual-input digitally driven Doherty amplifier architecture for performance enhancement of Doherty transmitters. *IEEE Trans Microw Theory Techn*, 59(5):1284-1293. https://doi.org/10.1109/TMTT.2011.2106137

de Falco PE, Mimis K, Ben-Smida S, et al., 2018. Single-ended branch PA characterisation for outphasing amplifiers. 13th European Microwave Integrated Circuits Conf, p.178-181. https://doi.org/10.23919/EuMIC.2018.8539963

Fang XH, Cheng KKM, 2014. Extension of high-efficiency range of Doherty amplifier by using complex combining load. *IIEEE Trans Microw Theory Techn*, 62(9):2038-2047. https://doi.org/10.1109/TMTT.2014.2333713

Fang XH, Liu HY, Cheng KKM, et al., 2018. Two-way Doherty power amplifier efficiency enhancement by incorporating transistors' nonlinear phase distortion. *IEEE Trans Microw Theory Techn*, 28(2):168-170. https://doi.org/10.1109/LMWC.2017.2783845

Gustafsson D, Andersson CM, Fager C, 2013. A modified Doherty power amplifier with extended bandwidth and reconfigurable efficiency. *IEEE Trans Microw Theory Techn*, 61(1):533-542. https://doi.org/10.1109/TMTT.2012.2227783

Hallberg W, Özen M, Gustafsson D, et al., 2016. A Doherty power amplifier design method for improved efficiency and linearity. *IEEE Trans Microw Theory Techn*, 64(12):4491-4504. https://doi.org/10.1109/TMTT.2016.2617882

Hasin MR, Kitchen J, 2019. Exploiting phase for extended efficiency range in symmetrical Doherty power amplifiers. *IEEE Trans Microw Theory Techn*, 67(8):3455-3463. https://doi.org/10.1109/TMTT.2019.2921366

Iwamoto M, Williams A, Chen PF, et al., 2001. An extended Doherty amplifier with high efficiency over a wide power range. *IEEE Trans Microw Theory Techn*, 49(12):2472-2479. https://doi.org/10.1109/22.971638

Kim B, Kim J, Kim I, et al., 2006. The Doherty power amplifier. *IEEE Microw Mag*, 7(5):42-50. https://doi.org/10.1109/MW-M.2006.247914

Kliks A, Kulacz L, Kryszkiewicz P, et al., 2020. Beyond 5G: big data processing for better spectrum utilization. *IEEE Veh Technol Mag*, 15(3):40-50. https://doi.org/10.1109/MVT.2020.2988415

Koenig S, Lopez-Diaz D, Antes J, et al., 2013. Wireless sub-THz communication system with high data rate. *Nat Photon*, 7(12):977-981. https://doi.org/10.1038/nphoton.2013.275

Lee J, Son J, Kim B, 2014. Optimised Doherty power amplifier with auxiliary peaking cell. *Electron Lett*,

50(18):1299-1301.
https://doi.org/10.1049/el.2014.2214

Lee SC, Paek JS, Jung JH, et al., 2015. 2.7 A hybrid supply modulator with 10dB ET operation dynamic range achieving a PAE of 42.6% at 27.0dBm PA output power. IEEE Int Solid-State Circuits Conf Digest of Technical Papers, p.1-3.
https://doi.org/10.1109/ISSCC.2015.7062916

Lehna R, Bangert A, 2016. Novel output combiner for three-way Doherty power amplifiers. 11th European Microwave Integrated Circuits Conf, p.137-140.
https://doi.org/10.1109/EuMIC.2016.7777509

Li C, You F, Peng J, et al., 2020. Co-design of matching sub-networks to realize broadband symmetrical Doherty with configurable back-off region. *IEEE Trans Circ Syst II Expr Briefs*, 67(10):1730-1734.
https://doi.org/10.1109/TCSII.2019.2946395

Li M, Li Z, Zheng Q, et al., 2022. A 17–26.5 GHz 42.5 dBm broadband and highly efficient gallium nitride power amplifier design. *Front Inform Technol Electron Eng*, 23(2):346-350.
https://doi.org/10.1631/FITEE.2000513

Liu X, Lv GS, Wang DH, et al., 2020. Energy-efficient power amplifiers and linearization techniques for massive MIMO transmitters: a review. *Front Inform Technol Electron Eng*, 21(1):72-96.
https://doi.org/10.1631/FITEE.1900467

Mustafa AK, Bassoo V, Faulkner M, 2009. Reducing the drive signal bandwidths of EER microwave power amplifiers. IEEE MTT-S Int Microwave Symp Digest, p.1525-1528.
https://doi.org/10.1109/MWSYM.2009.5165999

Nghiem XA, Negra R, 2014. Novel design of a 10 dB back-off broadband sequential Doherty power amplifier for wireless applications. IEEE Topical Conf on Power Amplifiers for Wireless and Radio Applications, p.22-24. https://doi.org/10.1109/PAWR.2014.6825735

Özen M, Andersson K, Fager C, 2016. Symmetrical Doherty power amplifier with extended efficiency range. *IEEE Trans Microw Theory Techn*, 64(4):1273-1284.
https://doi.org/10.1109/TMTT.2016.2529601

Pang JZ, He SB, Dai ZJ, et al., 2016. Design of a post-matching asymmetric Doherty power amplifier for broadband applications. *IEEE Microw Wirel Compon Lett*, 26(1):52-54.
https://doi.org/10.1109/LMWC.2015.2505651

Sen B, 2018. A 60W class S and outphasing hybrid digital transmitter for wireless communication. IEEE Topical Conf on RF/Microwave Power Amplifiers for Radio and Wireless Applications, p.8-11.
https://doi.org/10.1109/PAWR.2018.8310053

Suo HL, Bao JF, 2008. Three-way Doherty power amplifier with uneven power drive. 11th IEEE Int Conf on Communication Technology, p.293-296.
https://doi.org/10.1109/ICCT.2008.4716245

Tajima Y, Wandrei D, Schultz QS, et al., 2017. Improved efficiency in outphasing power amplifier by mixing outphasing and amplitude modulation. IEEE Topical Conf on RF/Microwave Power Amplifiers for Radio and Wireless Applications, p.55-58.
https://doi.org/10.1109/PAWR.2017.7875572

Tan C, Liu SW, Jia JB, et al., 2020. A wideband electrical impedance tomography system based on sensitive bioimpedance spectrum bandwidth. *IEEE Trans Instrum Meas*, 69(1):144-154.
https://doi.org/10.1109/TIM.2019.2895929

Vijarnstit P, Maneekut R, Kaewplung P, 2015. A flexible fiber access network using superchannel coherent optical orthogonal frequency division multiplexing. 17th Int Conf on Advanced Communication Technology, p.319-322. https://doi.org/10.1109/ICACT.2015.7224812

Wei LL, Hu RQ, Qian Y, et al., 2014. Key elements to enable millimeter wave communications for 5G wireless systems. *IEEE Wirel Commun*, 21(6):136-143.
https://doi.org/10.1109/MWC.2014.7000981

Zhou XY, Zheng SY, Chan WS, et al., 2018. Postmatching Doherty power amplifier with extended back-off range based on self-generated harmonic injection. *IEEE Trans Microw Theory Techn*, 66(4):1951-1963.
https://doi.org/10.1109/TMTT.2017.2784811